Influence of initial pressure on hydrogen/air flame acceleration during severe accident in NPP

R. Scarpa, E. Studer, S. Kudriakov, B. Cariteau, Nabiha Chaumeix

INFLUENCE OF INITIAL PRESSURE ON HYDROGEN/AIR FLAME ACCELERATION DURING SEVERE ACCIDENT IN NPP

Scarpa, R.[1], Studer, E.[2], Kudriakov, S.[3], Cariteau, B.[4] and Chaumeix, N.[5]
[1] DEN-STMF, CEA, Université Paris-Saclay, Gif-sur-Yvette, 91191, France, roberta.scarpa@cea.fr
[2] DEN-STMF, CEA, Université Paris-Saclay, Gif-sur-Yvette, 91191, France, etienne.studer@cea.fr
[3] DEN-STMF, CEA, Université Paris-Saclay, Gif-sur-Yvette, 91191, France, sergey.kudriakov@cea.fr
[4] DEN-STMF, CEA, Université Paris-Saclay, Gif-sur-Yvette, 91191, France, benjamin.cariteau@cea.fr
[5] ICARE, CNRS-Orléans, Avenue de la Recherche Scientifique, Orléans, 45100, France, chaumeix@cnrs-orleans.fr

ABSTRACT

Flame acceleration (FA) and explosion of hydrogen/air mixtures remain key issues for severe accident management in nuclear power plants. Empirical criteria were developed in the early 2000s by Dorofeev and colleagues, providing effective tools to discern possible FA or DDT (Deflagration-to-Detonation Transition) scenarios. A large experimental database, composed mainly of middle-scale experiments in obstacle-laden ducts at atmospheric pressure condition, has been used to validate these criteria. However, during a severe accident, the high release rate of steam and non-condensable gases into the containment can result in pressure increase up to 5 bar abs. In the present work, the influence of the unburnt gas initial pressure on flame propagation mechanisms was experimentally investigated. Premixed hydrogen/air mixtures with hydrogen concentration close to 11% and 15% were considered. From the literature, we know that these flames are supposed to accelerate up to Chapman-Jouguet deflagration velocity in long obstacle-laden tubes at initial atmospheric conditions. Varying the pressure in the fresh gas in the range 0.6-4 bar, no effects on the flame acceleration phase were observed. However, as the initial pressure was increased, we observed a decrease in the flame velocity close to the end of the tube. The pressure increase due to the combustion reaction was found to be proportional to the initial pressure according to adiabatic isochoric complete combustion.

NOMENCLATURE

Latin letters

AICC	Adiabatic Isochoric Complete Combustion	
BR	Blockage ratio	[-]
c	Speed of sound	[m/s]
CC	Piezoelectric shock sensor	
CJ	Chapman-Jouguet condition	
d	Obstacle inner diameter	[m]
D	Inner tube diameter	[m]
DDT	Deflagration-to-Detonation Transition	
f	Frequency	[Hz]
FA	Flame Acceleration	
l	Tube length	[m]
L_T	Turbulent mixing length	[m]
Le	Lewis number	[-]
n	Overall reaction order	[-]
p	Pressure	[bar]
PP	Piezoelectric pressure sensor	

PMT	Photomultiplier tube	
S	Fundamental flame speed	[m/s]
T	Temperature	[K]
V	Velocity	[m/s]
x	Distance	[m]

Greek letters

α	Thermal diffusivity	[m^2/s]
β	Zeldovich number	[-]
χ	Molar fraction	[-]
δ	Flame thickness	[m]
ϕ	Equivalence ratio	[-]

Superscripts and subscripts

0	Initial condition
a	Acoustics
ad	Adiabatic combustion
b	Burnt gas
c	Cut-off
def	Deflagration
det	Detonation
F	Flame
H_2	Hydrogen
L	Laminar
max	Maximum
s	Sound
S	Shock
u	Unburnt gas

1.0 INTRODUCTION

In case of severe accident, in-core metal-water reactions due to fuel heat-up lead to massive release of hydrogen into the containment of Light Water Reactors, as recently recalled by Fukushima accident. The safety features currently implemented for severe accident management do not avoid the possible formation of large flammable clouds. If ignited, hydrogen/air flames may accelerate up to supersonic speeds over a wide range of hydrogen concentration. Such explosions could eventually jeopardize the integrity of the containment and damage components important to safety or accident management. The structural damage depends on the maximum pressure but also on the pressure impulse [1]. Therefore, they are more important when the propagation velocity of the reactive wave increases.

The empirical flame acceleration criteria developed in the early 2000s by Dorofeev and colleagues [2], [3] provide effective tools for the analysis of the possible scenarios and it allows the selection of the most relevant situations for which flame acceleration (FA) may take place. Nevertheless, most of FA and DDT (Deflagration-to-Detonation Transition) criteria are based on experimental databases in which explosions were carried out at atmospheric conditions. In case of a severe accident, the high release rate of steam and non-condensable gases into the containment may result in a pressure increase up to 5 bar abs. Therefore, hydrogen explosions are more likely to happen at an initial pressure greater than the atmospheric one.

According to the thermal theory of Mallard and Le Chatelier, the laminar burning velocity is expected to vary in line with expression (1):

$$S_L \propto p^{\frac{n-2}{2}}, \quad (1)$$

where $n = n(p)$ is the overall reaction order. For lean mixtures at atmospheric conditions $n \leq 1$, therefore S_L decreases with increasing pressure. This variation is linked to the fact that the ignition temperature tends to increase as the initial pressure increases. According to [4], n strongly decreases with pressure and for lean mixtures it may reach negative values. In Fig.1 the variation of the laminar burning velocity with pressure for 11 and 15 %vol H_2-air mixture are shown. COSILAB® v.3 code [5], coupled with the detailed kinetic mechanism described in [6], was used to compute the laminar flame speed. In the literature, we found four references dealing with the effect of initial pressure on the laminar flame velocity of a hydrogen/air mixture at room temperature [9], [10], [11] and [12]. At 11 vol%, the calculations underestimate the experimental results by a factor of about 3 at 1 bar. Nevertheless, the trends are the same as when the pressure increases the velocity decreases. These deviations can be explained by the difficulty of experimentally overcoming the intrinsic instabilities of the flame or by a weak kinetic scheme for these low flame temperatures. At 15 vol%, this underestimation is reduced to a factor of 2. However, the results of Kitagawa et al correspond well to the simulation and those of Aung et al show a singular behavior for pressures above twice the atmospheric pressure. At this hydrogen content, the flames are less unstable. For lean flames below equivalent ratio of 0.8, it is impossible to get rid of flame wrinkling and now it is often proposed to validate kinetic models above and then extrapolate. Nevertheless, if we look at the data collected by [13] for hydrogen/air mixtures under ambient temperature and pressure conditions, values between 25 and 35 cm/s for 15 vol% and between 5 and 15 cm/s for 11 vol% were obtained. Our computed results are consistent with these data.

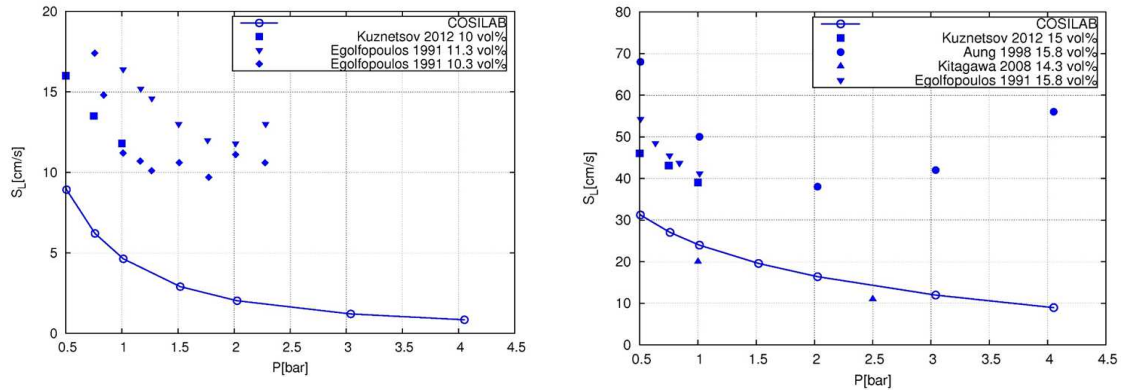

(a) (b)

Figure 1. Laminar burning velocity vs. pressure: (a) 11 %vol H_2-air mixture (ϕ = 0.296), (b) 15 %vol H_2-air mixture (ϕ = 0.422).

For lean mixture at $p < 10$ bar the activation energy increases as $p^{0.5}$. Since the adiabatic flame temperature is essentially independent of pressure in the range of pressure variation considered in the present study, the Zeldovich number β is supposed to vary in the same way as the activation energy. Moreover, by assuming that $T_{b,ad}$ remains constant, we make the hypothesis that the speed of sound in the burnt gas is not affected by pressure variations.

In the present work, the influence of p_0 on premixed hydrogen/air flame propagation has been experimentally investigated in the SSEXHY facility (Structures Submitted to an EXplosion of HYdrogen). The device (Fig. 2) consists of a stainless steel tube equipped with annular obstacles

uniformly distributed all along the tube length. Experiments were performed at initial pressure in the range 0.6-4 bar abs. For this campaign, we chose to test mixtures with hydrogen content close to 11.0 %vol. From literature [7] we know that these mixtures are supposed to accelerate inside an obstacle-laden tube up to an asymptotic velocity. This saturation velocity corresponds to the Chapman-Jouguet deflagration speed [8]. By decreasing the hydrogen concentration, the mixture is shown to be not sufficiently energetic to sustain the above mentioned condition. As a result, these flames may be partially or totally quenched depending on the obstacle blockage ratio. At atmospheric initial conditions, mixtures with 11.0 %vol hydrogen identify the lower limit for FA [3]. In consequence, their behavior is quite unstable: even the slightest variation of a fundamental parameter may lead to significant modification of flame behavior.

2.0 EXPERIMENTAL SETUP

The experimental facility (Fig. 2 and Fig. 3) is an obstacle-laden tube designed to study the acceleration mechanisms of premixed hydrogen/air flames. The tube is composed of 4 modules of the same length $l = 1310$ mm and internal diameter $D = 120$ mm. In the present experimental campaign only three modules are exploited for a total length of 3930 mm. If this study had focused on the chocked flame regime it would have been more appropriate to use four sections. As the acceleration profile was the goal of this work, the three sections provided enough information.

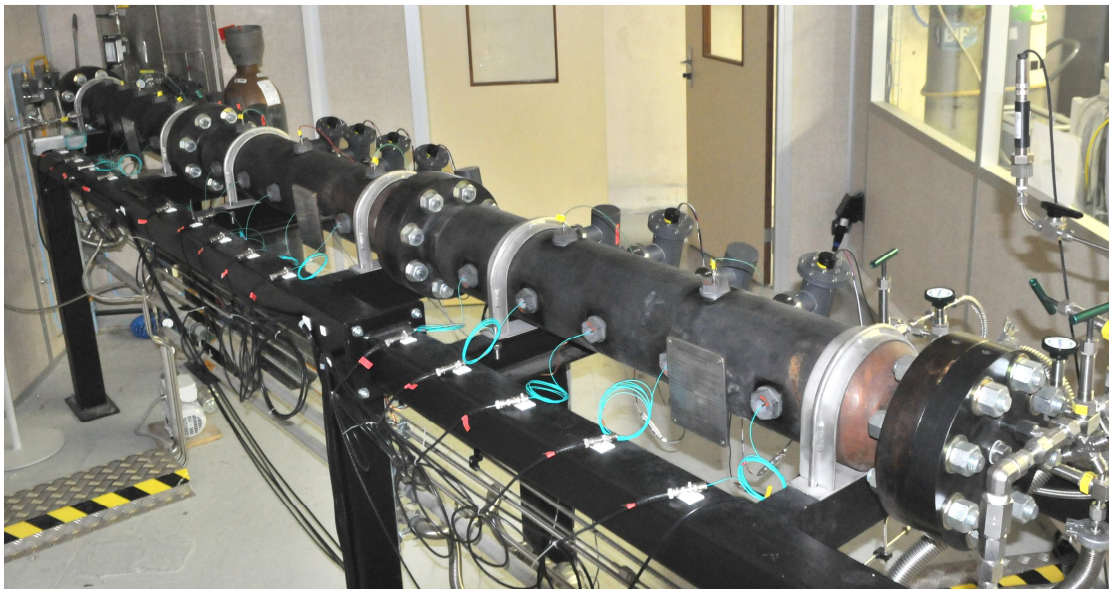

Figure 2. SSEXHY facility in the 3-modules configuration.

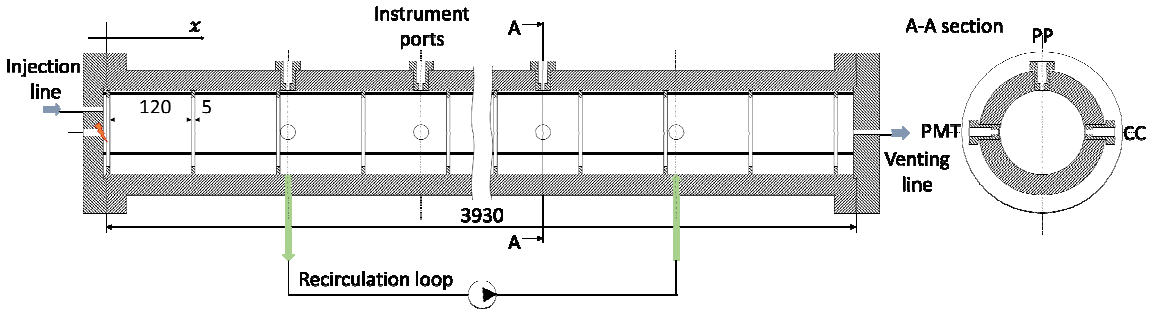

Figure 3. Schematic of the experimental device. Lengths are given in mm.

The acceleration tube is designed for a nominal operating pressure of 100 bar, making the device suitable for studying both deflagration and detonation mechanisms. Gas injection and venting lines are located at the flanged heads. The first head also hosts in its centre an automotive spark plug used to ignite the flammable mixture, as shown in Fig. 3.

Thirty-two equally spaced annular obstacles have been installed inside the tube with the aim of promoting turbulence at the wall. Obstacle blockage ratio ($BR = 1 - (d/D)^2$) is equal to 0.3. Three thin threaded rods form the structure supporting the obstacles. The stainless steel annular obstacles (5 mm thick) present three holes, 120° spaced from each other, for rods insertion. Obstacles are 120 mm spaced from each other, resulting in a 125 mm uniform pitch.

Air (20.1% O_2 – 70.9% N_2) and hydrogen are consecutively injected into the tube from two separated gas tanks. Prior to gas injection, lines are vented by removing the residual gas with a vacuum pump, thus avoiding any contact between hydrogen and oxygen. This precaution allows us to achieve a flammable mixture only inside the tube. At the end of the injection process, the injection system is inerted with nitrogen. Hydrogen concentration can be varied inside flame propagation limits, covering the whole spectrum of possible mixtures from lean mixtures to rich ones, including stoichiometric conditions. Once the initial conditions of the experiment are established, i.e. pressure and hydrogen concentration, the method of partial pressures is used to prepare the desired mixture inside the tube. Three pressure sensors are available for three different pressure ranges: a vacuum gauge in the range 0-133 mbar, a pressure transmitter in the range 0-1000 mbar, while the last one covers the range 0-5 bar.

Since hydrogen and air are injected at different times, a concentration gradient is formed along the tube axis. An ATEX gas recirculation pump then promotes mixture homogenisation. The mixture is forced to recirculate into an external loop for about 30 minutes before reaching the homogeneous condition. This period of time was calibrated from pre-tests using helium instead of hydrogen and measuring the local concentration with thermal conductivity gauges. Close to the recirculation loop entrance at the tube wall, two taps are available for gas sampling. Gas samples are then analysed by a gas chromatograph (Agilent 490 μGC). The uncertainty in gas composition is in the order of 0.1 %vol.

In the 3-modules configuration, the combustion tube is equipped with 40 instrumentation ports. The instrumentation configuration for the present experimental campaign involved fourteen photomultiplier tubes (PMT), nine piezoelectric pressure sensors (PP) and fourteen piezoelectric shock sensors (CC). Sensors disposition along the tube is detailed in Tab. 1. Here the origin $x = 0$ corresponds to the inner surface of the first flanged connection, located 5 mm away from the origin of the fluid domain, as shown in Fig. 3.

Table 1. Instrumentation configuration.

Location [mm]	Shock sensors	Pressure sensors (type)	Photomultiplier tubes
265			PMT1
460	CC1	PP1 (6001)	PMT2
655	CC2	PP2 (7001)	PMT3
850	CC3	PP3 (6001)	PMT4
1045	CC4	PP4 (601A)	PMT5
1575	CC5	PP5 (7001)	PMT6
1770	CC6		PMT7
1965	CC7	PP6 (7001)	PMT8
2160	CC8		PMT9
2355	CC9	PP7 (7001)	PMT10
2885	CC10		PMT11
3080	CC11	PP8 (7001)	PMT12

3275	CC12		PMT13
3470	CC13	PP9 (7001)	PMT14
3665	CC14		

A cross sectional view of the tube shows the position of the sensors on the tube diameter (A – A section in Fig. 3). On the vertical position (on the top generatrix of the tube) we can find dynamic pressure sensors (Kistler 601A, 6001 and 7001 types). For the 601A and 6001 types we have used a flush mounting nut, while 7001 type are recessed mounted. At 90° from the pressure sensors, we can find the optical access for the Hamamatsu R11568 photomultiplier tubes (PMT). These detectors collect the UV light emitted by $OH^{\bullet}$ radicals located at the reaction front within a very narrow solid angle (the uncertainty on the flame position for the collimated beam is $\delta x_{\max} = 3.66\,\text{mm}$). As the flame tip passes through the PMT solid angle, a negative voltage is recorded. This signal allows us to extrapolate the time-of-arrival of the flame tip, monitoring flame propagation along the tube axis.

On the other side, Chimiemetal piezoelectric sensors are located. These detectors allow the detection of a shock wave in the unburnt gas. Thanks to their small sensitive area (2 mm diameter), they can be used to extrapolate the velocity of the pressure wave ahead of the flame in a more accurate way. These sensors are not calibrated and strongly affected by the radiation emitted by the flame. As a result, once the flame passes by the sensor, the piezoelectric crystal respond with a strong current pulse. Their use is therefore restricted to the detection of the shock waves ahead the flame, in the unburnt gas.

Tube inner wall, as well as obstacles surface, was thermally treated with black oxides to prevent light reflection. The accuracy of optical measurements is therefore increased.

National Instrument NI PXIe-1078 data acquisition station was used to record sensors output signals. The five data acquisition cards 12-bit, 8-channels NI PXIe-5105 (with onboard memory) allow a maximum record frequency of 60 MHz per card. Acquisition trigger and signal record are controlled via LabVIEW 2015 platform. The program is coded to launch signal acquisition as the ignition spark is initiated.

3.0 RESULTS AND DISCUSSION

Test conditions are presented in Tab. 2. A repeatability study was performed at $p_0 = 1$ bar in order to compare the results obtained in the present work with those from literature. In Fig. 4(a) the velocity of the flame tip along the tube axis is presented for the test cases 3, 4 and 5 ($\chi_{H_2} \approx 11\%$). Present results were compared to those from [7] for the same mixture composition and obstacle blockage ratio.

In Fig. 4(a) the error band associated to velocity measurement technique is also presented for the three test cases. This uncertainty is related to the error in the flame position measurement introduced by PMT solid angle. In Fig. 4(b) a repeatability study for $\chi_{H_2} = 14.5\%$ is presented. Here the error band represents minimum and maximum values over three repeated shots.

Table 2. Test matrix.

Test #	p_0 [mbar]	χ_{H_2} [%]	Test #	p_0 [mbar]	χ_{H_2} [%]
1	600	10.9	11	600	14.8
2	800	11.1	12	600	14.4
3	1000	11.1	13	1000	14.6
4	1000	11.2	14	1000	14.6
5	1003	10.9	15	1000	14.9
6	1501	11.1	16	1001	15.0
7	1502	10.9	17	1002	14.8

8	2000	11.1	18	2000	14.6
9	4002	11.1	19	4001	14.4

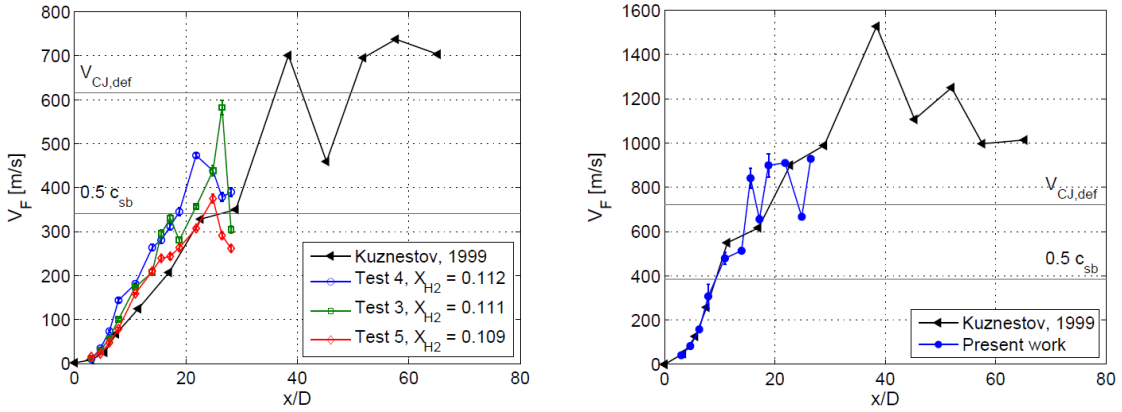

(a) $\chi_{H_2} \approx 11\%$. (b) $\chi_{H_2} = 14.5\%$.

Figure 4. Repeatability study at atmospheric pressure ($p_0 = 1000$ mbar). Experiments performed during the present work are compared to those from [7] for the same mixture composition and obstacle blockage ratio.

The experiments performed with a more reactive mixture match perfectly the data presented in [7], while for mixtures with 11% hydrogen data dispersion is wider. These flames show in fact a quite unstable behaviour that reflects in the repeatability study. As shown in Fig. 4(a), the experimental device is not long enough to allow the flame to reach the CJ deflagration velocity for a 11 %vol hydrogen mixture.

Sensors output signals were recorded at 100 kHz. To eliminate the noise related to electronics and structures resonance, a low-pass filter was applied to the signals. The cut-off frequency was chosen to preserve burnt gas acoustics among the obstacles. The frequency of an acoustic wave propagating in the burnt gas inside the chamber delimited by two obstacles can be computed as follows:

$$f_a = \frac{c_{sb}}{2D}. \tag{2}$$

For 11% hydrogen, $c_{sb} = 684$ m/s thus $f_a = 2850$ Hz. The cut-off frequency for the filtering process was then imposed to be $f_c \geq f_a$. To avoid damping the amplitude of those harmonics close to f_a, we decided to use $f_c = 3200$ Hz.

In Fig. 5, signals from Test 1 are presented in a 70 ms time window. Since the acquisition is triggered by the current that supplies the electrical spark, the exact time t_0 at which the ignition of the mixture takes place is unknown. In the graph, signals are plotted according to their non-dimensional position x/D along the tube. The solid large black lines identify tube modules borders. Both recorded pressure signals (light grey lines) and filtered ones (red lines) are presented in Fig. 5. Signals recorded by piezoelectric sensors correspond to the dynamic overpressure. The absolute pressure can then be obtained by adding to the overpressure the initial value of the pressure. An important thing to point out is that the radiation emitted by the flame strongly influences the response of those pressure sensors in flush mounting position (PP1, PP3 and PP4). By comparing PP2 and PP3 signals, we can note that the sensor in the recessed mounting position undergoes a lower thermal load.

The time-of-arrival diagram of the flame tip, drawn from photomultiplier tubes response, is also presented in Fig. 5 with a blue solid curve. For the sake of clarity, shock sensor output signals are not presented in the graph.

The saw-tooth shape of the pressure signals visible in Fig. 5 is caused by the shock waves reflecting on the head flanges. For the test cases with $p_0 \leq 1000$ mbar, a quasi-mono-dimensional leading shock is formed. Post-processing pressure signals from Test 1, we found that, after the first reflection at the end of the tube, the shock wave propagates at almost 701 m/s. At each reflection, its velocity decreases: $V_S = 655$ m/s after the second reflection, $V_S = 630$ m/s after the third one, $V_S = 594$ m/s after the fourth one and so on. The shock wave is therefore less energetic at each step. Decaying speed of sound 701, 655, 630, 594 m/s correspond to the average temperature for combustion products 1220, 1060, 980, 875K, respectively, decaying due to energy losses. As the initial pressure is increased, the leading shock wave can no longer be considered mono-dimensional. As a result, pressure signals are characterized by a multitude of peaks with the same frequency (corresponding to a sound wave travelling along the tube) but different phase (see Fig. 7(a) and Fig. 8(a)).

The influence of the initial pressure on the flame velocity is shown in Fig. 6. For the leanest mixture, test cases were sorted in two groups depending on the hydrogen concentration. In Fig. 6(a) we present the test cases with $\chi_{H_2} = 10.9\%$, while in Fig. 6(b) those cases with $\chi_{H_2} = 11.1\%$ are shown.

For 11% in air, in the first stage of flame acceleration no significant differences with pressure variation were observed. Measurement spread is in fact comparable to that one shown in the repeatability study. Thus, even if the laminar burning velocity decreases of a factor 9 from 0.6 bar to 4 bar, as shown in Fig. 1, it seems to have little influence on the first phase of flame acceleration. However, the burning rate $\rho_u S_L$ (Fig. 6(d)) is indicative of the rate of consumption of the fresh gases and it decreases slightly when the pressure increases. There are therefore other parameters relevant for the flame acceleration mechanism that intervene in compensating the decrease in burning rate. Moreover, these flames are thermally unstable. Since the Lewis number is an invariant of pressure, Le~ const~0.347, the product β(Le-1) is always negative and lower than the threshold stability value -2.

In Fig. 6(c) the effect of initial pressure on flame velocity for hydrogen/air mixture with 15 vol% is presented. For p_0= 0.6 and 1 bar, the velocity profiles are perfectly superposed up to x/D=15 despite a large variation of the burning rate. For p_0 greater than 2 bar, instead, a greater acceleration rate is observed from the early stages of flame acceleration. As pointed out in Fig. 6(c) the burning rate continues to rise and at the same time the product β(Le-1) becomes even more negative. It seems that it is mainly the initial phase, which is faster, and therefore this acceleration can be mainly attributed to the variations of the thermodiffusive parameters.

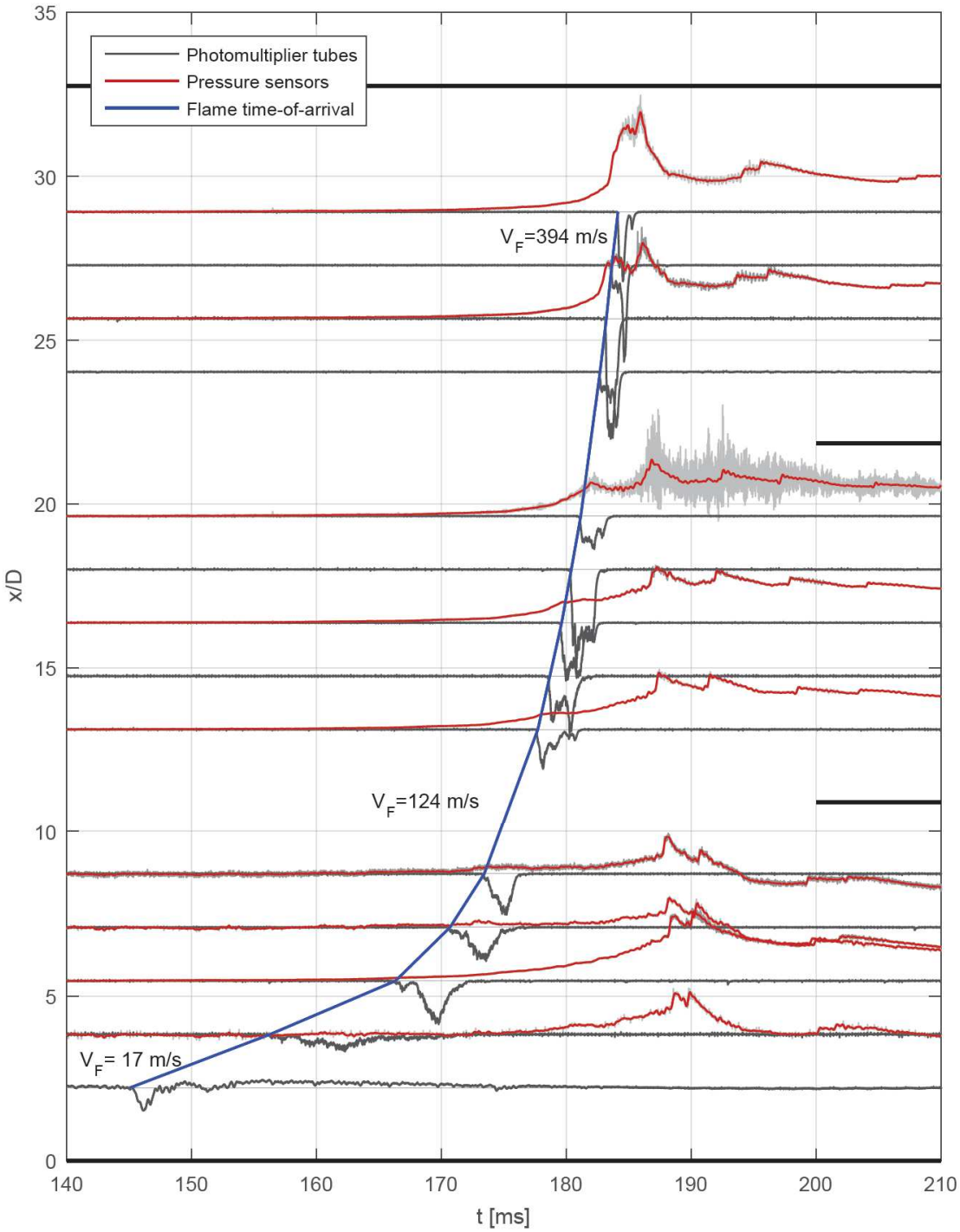

Figure 5. Test 1: $p_0 = 600$ mbar and $\chi_{H_2} = 0.109$. Cut-off frequency on pressure sensors output signal $f_c = 3200$ Hz.

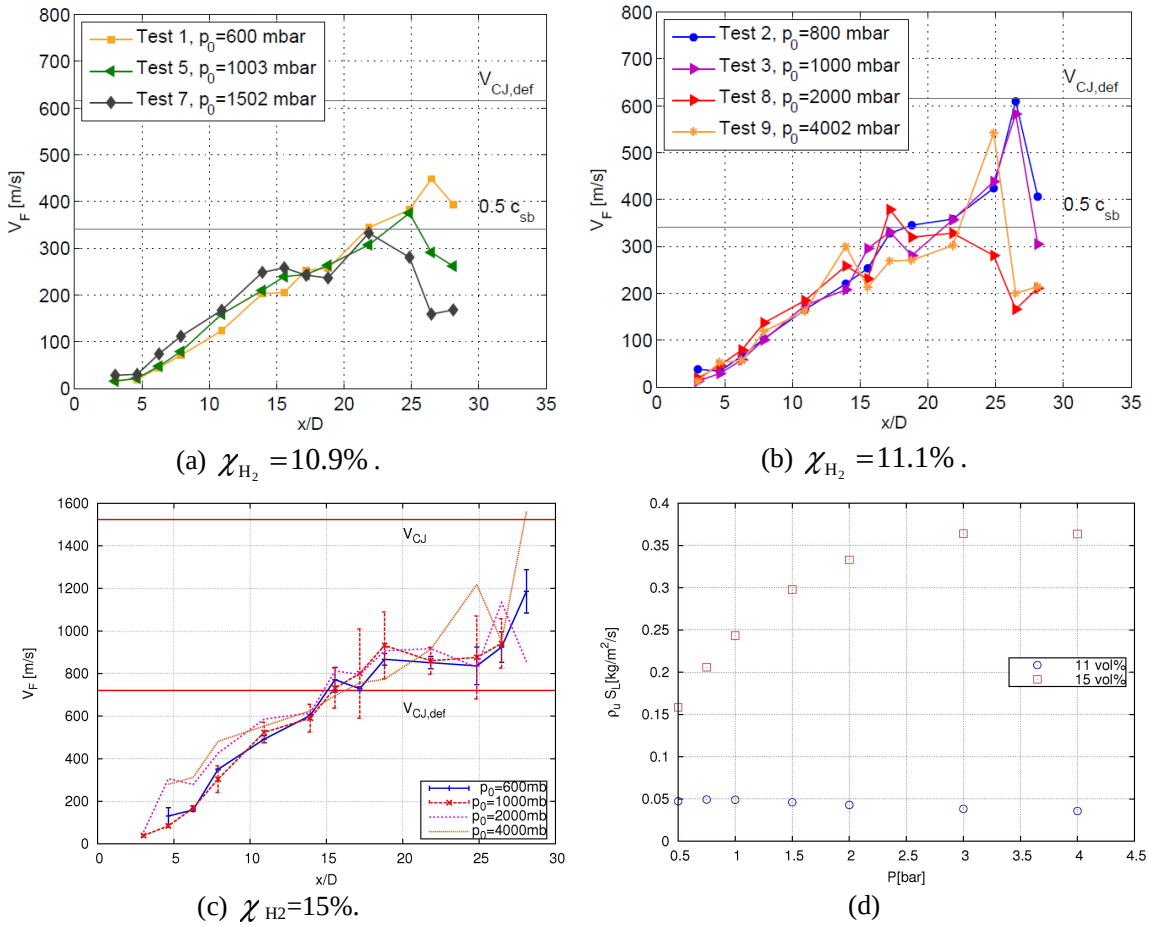

(a) $\chi_{H_2} = 10.9\%$. (b) $\chi_{H_2} = 11.1\%$.

(c) $\chi_{H2} = 15\%$. (d)

Figure 6. Flame tip velocity (a), (b) and (c), computed burning rate (d).

The σ-criterion described in [3] is satisfied for all the cases considered in this work. This criterion identifies a necessary condition for flame acceleration for a given mixture and geometry. According to [7], at large scale the threshold value σ^* depends only on the mixture composition and the initial conditions. This limit is defined by the condition $L_T / \delta \geq 100$, where L_T is the integral mixing length and δ is the flame thickness. The expansion ratio, σ, does not depend on pressure and, for a mixture with 11 %vol hydrogen, its value coincide with the threshold value for FA found by Dorofeev and colleagues at atmospheric condition, $\sigma^* = 3.7$. Nevertheless, in our experiments, by increasing the initial pressure, the ratio L_T / δ decreases, as shown in Fig. 7. Here, the definitions given in [3] were used to compute the integral mixing length and the flame thickness:

$$L_T = D \tag{3}$$

$$\delta = \frac{\alpha(T_b)}{\sigma S_L}, \tag{4}$$

where $\alpha(T_b)$ is the thermal diffusivity in the burnt gas. For $L_T / \delta < 100$, the geometry plays an important role in the flame propagation mechanism. By increasing the turbulence of the gas flow ahead of the flame, flame stretching may then cause flame slowdown or extinction. As shown in Fig. 6, the last stage of flame propagation (starting approximately with the 20th obstacle) is characterized by a decrease of flame velocity. This slowdown is more pronounced as the initial pressure increases. Anyway, global flame quenching did not occur. At the end of the tube, the flame front is also

perturbed by the reflected pressure wave. As the reflected shock interacts with the flame, hydrodynamic forces tend to slowdown the flame.

Fig. 8 and Fig. 9 show the pressure variations recorded by PP6 and PP9 for different tests. In these pipe sections (Fig 3 right), a PMT is associated with a pressure sensor. In order to compare the pressure measurements, curves are shifted in time based on PMT time-response at the correspondent pressure sensor position. Flame tip time-of-arrival is also presented in the graphs with a vertical black line.

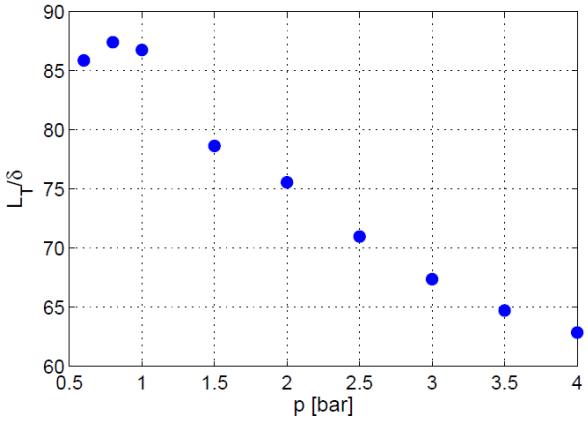

Figure 7. L_T / δ vs. pressure for 11 %vol H2-air mixture.

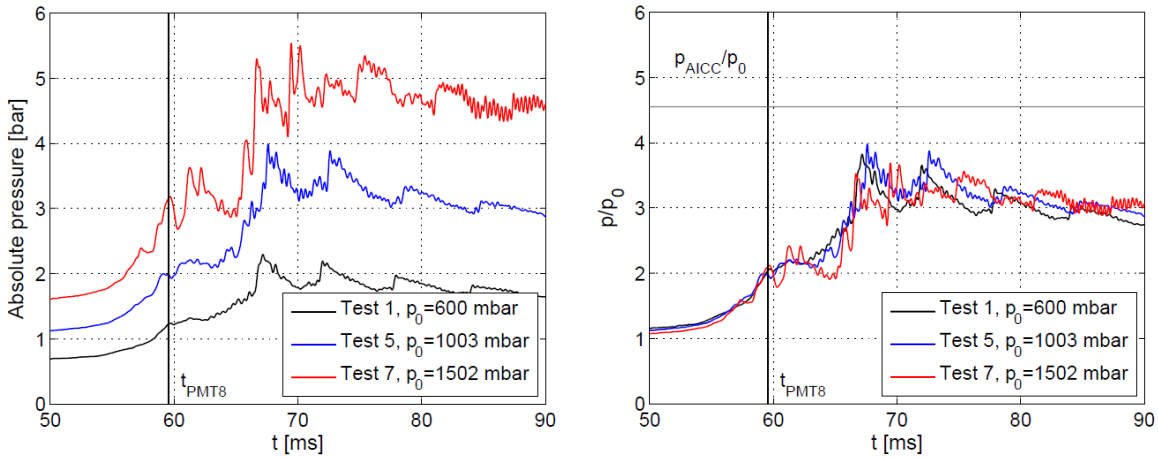

(a) (b)

Figure 8. Influence of the initial pressure p_0 on the pressure peaks recorded by PP6: (a) absolute pressure; (b) absolute pressure to initial pressure ratio.

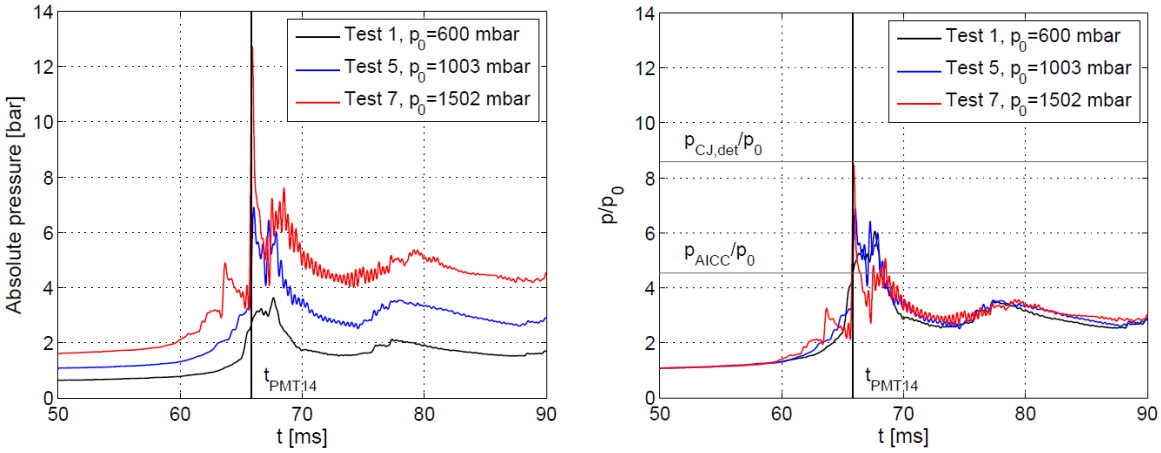

(a) (b)

Figure 9. Influence of the initial pressure p_0 on the pressure peaks recorded by PP9: (a) absolute pressure; (b) absolute pressure to initial pressure ratio.

As the initial pressure is increased, the signals show a more oscillating profile. The frequency of these oscillations matches f_a. Then, the amplitude of acoustic waves in the burnt gas becomes more important as the initial pressure increases. In Fig 8(b) and Fig. 9(b), the absolute pressure to the initial pressure ratio is presented.

From the graphs, we can state that the pressure increase due to the combustion reaction is directly proportional to the initial pressure according to adiabatic isochoric complete combustion pressure (AICC). For completeness, the values of the adiabatic isochoric combustion pressure p_{AICC} and of the CJ detonation pressure $p_{CJ,\det}$ are also presented in Fig 8(b) and Fig. 9(b).

Finally, in Fig. 10 the pressure evolution recorded for test case 5 by the sensors located at the end of the tube is shown. We can see that shock sensors response is coherent with pressure sensors one. The pressure increase at the end of the tube is also consistent with an adiabatic isochoric complete combustion, as above mentioned. Additionally, the propagation of a reflected shock wave moving at the speed of sound in the burnt gas is traced with a purple line. In its way back, this wave further compresses the burnt gas. As a consequence, OH^* radicals population in the exited state increases. The photomultiplier tubes capture the light emitted during the transition to the ground state. As a result, in Fig. 10 PMT signals are characterized by the presence of an additional peak, of significantly lower amplitude if compared to the first one.

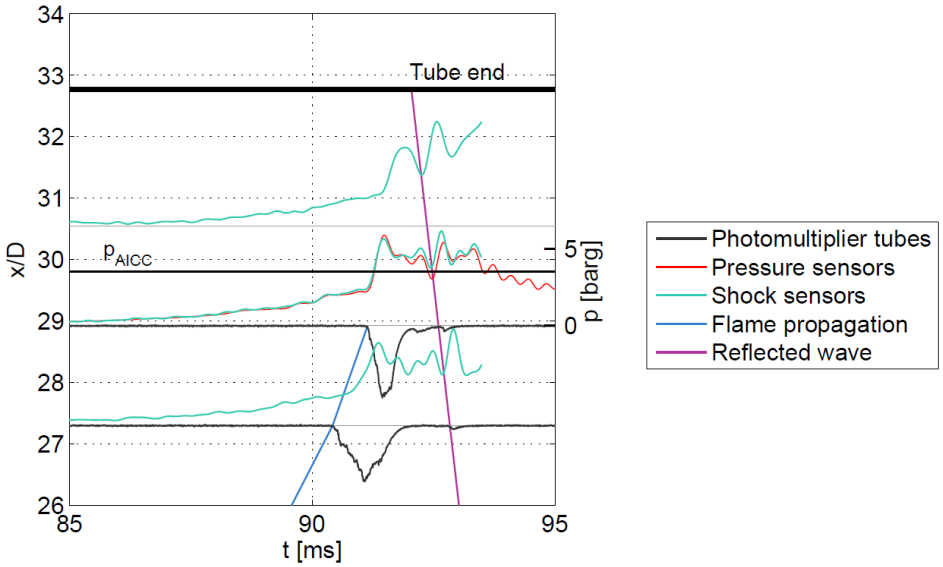

Figure 10. Test 5: $p_0 = 1003$ mbar and $\chi_{H_2} = 0.109$.

4.0 CONCLUSIONS

The effect of initial pressure on lean hydrogen/air flame acceleration was experimentally investigated. The initial pressure was varied in the rage 0.6-4 bar abs. In the early stages of flame acceleration, no significant changes were observed except for 15 vol% at 2 bar. In the central module, where the velocity increase is almost constant, a wide data dispersion was noticed for the leanest mixture. However, this spread is similar to that one encountered in the repeatability study. Therefore, even if the laminar burning velocity decreases of almost one order of magnitude from 0.6 bar to 4 bar, as shown in Fig. 1, it seems to have little influence on the first phase of flame acceleration.

As the initial pressure was increased, we observed a decrease in the flame velocity close to the end of the tube. The reason of this flame slowdown is mainly due to the interaction between the reflected shock wave and the flame. Fig. 7(b) and Fig. 8(b) show that the pressure increase due to the combustion reaction is directly proportional to the initial pressure. Therefore, the hydrodynamic force generated by the shock and acting on the flame becomes stronger, slowing down the flame in its propagation along the tube.

Further experimental campaigns are planned to complete the study. For these new experiments, we envisage to investigate the influence of the initial pressure on different mixture compositions, including rich mixtures. Obstacle size variation is also foreseen. In future works, the effect of the dynamic pressure peaks on simple stainless steel structures, such as plates and cylinders, placed at the end of the accelerating tube will also be analysed. A visualization module with quartz windows will be also available to perform optical flame front tracking measurements.

Present and future studies provide a solid base of experimental data for the validation of CFD models devoted to the simulation of LWR severe accident scenarios.

ACKNOWLEDGMENTS

The work was performed at the French Alternative Energies and Atomic Energy Commission (CEA). Authors thank Air Liquide and EDF for supporting current works.

REFERENCES

1. The Steel Construction Institute, Protection of piping systems subject to fires and explosions, Health &Safety Executive, 2005.
2. Breitung, W., Chan, C., Dorofeev, S. B., Eder, A., Gelfand, B., Heitsch, M., Klein, R., Malliakos, A., Shepherd, E., Studer, E. and Thibault, P., State-of-the-art report on flame acceleration and deflagration-to-detonation transition in nuclear safety, Nuclear Energy Agency, NEA/CSNI/R(2000)7
3. Dorofeev, S. B., Kuznetsov, M. S., Alekseev, V. I., Efimenko, A. and Breitung, W., Evaluation of limits for effective flame acceleration in hydrogen mixtures, *J. Loss Prev. Process Ind.*, **14**, 2001, pp. 583–589.
4. Law, C. K., Propagation, structure, and limit phenomena of laminar flames at elevated pressures, *Combustion Science and Technology*, **178**, 2006, pp. 335-360.
5. Rotexo. COmbution SImulation LABoratory. http://www.rotexo.com, 2015. [Online accessed 10-September-2015].
6. Connaire, M. O., Curran, H J., Simmie, J. M., Pitz, W. J. and Westbrook, C.K., A Comprehensive Modeling Study of Hydrogen Oxidation, *International Journal of Chemical Kinetics*, **36**, 2004, pp. 603-622.
7. Kuznetsov, M. S., Alekseev, V., Bezmelnitsyn, A. V., Breitung, W., Dorofeev, S. B., Matsukov, I., Vaser, A. and Yankin, Y. G., Effect of obstacle geometry on behaviour of turbulent flames, Forschungszentrum Karlsruhe, Technik und Umwelt, Report No. IAE-6137/3 FZKA 6328
8. Chue, R. S., Clarke, J. F. and Lee, J. H., Chapman-Jouguet deflagrations, *Proceedings of the Royal Society of London Series a-Mathematical Physical and Engineering Sciences*, **441**, No. 1913, 1993 pp. 607–623.
9. M. Kuznetsov, S. Kobelt, J. Grune, and T. Jordan, "Flammability limits and laminar flame speed of hydrogen-air mixtures at sub-atmospheric pressures," *Int. J. Hydrog. Energy*, vol. 37, pp. 17580–17588, 2012.
10. K. T. Aung, M. I. Hassan, and G. M. Faeth, "Effects of pressure and nitrogen dilution on Flame/Stretch interactions of laminar premixed H2/O2/N2 Flames," *Combust. Flame*, vol. 112, pp. 1–15, 1998.
11. T. Kitagawa, T. Nakahara, K. Maruyama, K. Kado, A. Hayakawa, and S. Kobayashi, "Turbulent burning velocity of hydrogen-air premixed propagating flames at elevated pressures," *Int. J. Hydrog. Energy*, vol. 33, pp. 5841–5849, 2008.
12. F. N. Egolfopoulos and C. K. Law, "An experimental and computational study of the burning rates of ultra-lean to moderately-rich H2/O2/N2 laminar flames with pressure variations," in *23rd Symposium on Combustion, The Combustion Institute*, 1990, pp. 333–340.
13. M. C. Krejci, O. Mathieu, A. J. Vissotski, S. Ravi, T. G. Sikes, E. L. Petersen, A. Kermones, W. Metcalfe, H. J. Curran, "Laminar Flame Speed and Ignition Delay Time Data for the Kinetic Modeling of Hydrogen and Syngas Fuel Blends", *J. Eng. Gas Turbines Power*, vol. 135, issue 2, 021503, 2013, 9 pages.